Available online at www.sciencedirect.com
SCIENCE DIRECT®
International Journal of Thermal Sciences 45 (2006) 537–552
International Journal of Thermal Sciences
www.elsevier.com/locate/ijts

Direct imaging of turbid media using long-time back-scattered photons, a numerical study

Joan Boulanger [a], Azad El Akel [b], André Charette [b,*], Fengshan Liu [a]

[a] *Groupe de Recherche en Ingénierie des Procédés et Systèmes, Département des Sciences Appliquées, Université du Québec à Chicoutimi, 555 Boulevard de l'Université, Chicoutimi, PQ, Canada G7H 2B1*
[b] *Technologie de la Combustion, Institut de Technologie des Procédés Chimiques et de l'Environnement, Conseil National de Recherche du Canada, 1200 Chemin de Montréal, Ottawa, ON, Canada K1A 0R6*

Received 9 November 2004; received in revised form 5 September 2005; accepted 26 September 2005

Available online 3 November 2005

Abstract

Direct imaging is a convenient way to obtain information on the interior of a semi-transparent turbid material by non-invasive probing using laser beams. The major difficulty is linked to scattering which scrambles the directional information coming from the laser beam. It is found in this paper that the long-term multiple-scattered reflected photons may provide structural information on the inside of a material, which offers an interesting alternative to using information only from un-scattered or least-scattered photons as obtained from current direct imaging set-ups for thin media.

Based on some observations on a non-homogeneous three layered 1-D slab irradiated by a laser pulse, a direct probing methodology making use of the long-term back-scattered photons is illustrated to recover inclusions positions in a turbid 2-D medium. First, the numerical model is presented. Second, an extended parametrical study is conducted on 1-D homogeneous and non-homogeneous slabs with different laser pulse durations. It is found that the reflected asymptotic logarithmic slope carries information about the presence of the inclusion and that short laser pulses are not necessary since only the decaying parts of the remanent optical signature is important. Longer laser pulses allow a higher level of energy injection and signal to noise ratio. Third, those observations are used for the probing of a 2-D non-homogeneous phantom.

Keywords: Direct imaging; Back-scattered photons; Near infrared radiation; Optical tomography; Biomedical optics; Discrete ordinates method; Transient radiation

1. Introduction

Optical tomography is viewed as a potential tool for non-invasive mapping of optical parameters in a semi-transparent material. Biomedical optics is occupying an increasing part of this field of applied optics research [1–3]. The main goal of biomedical optics is the development of a diagnostic imaging device based on near infra-red (NIR) radiation. Several improvements are expected over other imaging tools. First, repeated use of optical diagnostic presents no harm to the patient, since radiations utilized are non-ionizing. Second, in the case of some particular set-ups, such as inverse imaging, absorption and scattering may be recovered, providing not only structural but functional imaging such as identification of tissues or physiological changes due to pathology, e.g. [4,5]. Some applications of this new imaging method are presently in use and concern the monitoring of cerebral blood and tissue oxygenation [6]. Interesting elements may be found in the discussion review of reference [7].

Direct imaging uses transmitted light across materials to recover the internal structure through back-projection methods as in [8], where cerebral haemoglobin concentrations are monitored. However, direct transillumination of high scattering materials such as human tissues is of limited interest: multiple scattered photons provide only extremely blurred images. In reference [9], an estimation of scattering is given for a broad variety of biological tissues and the orders of magnitude show

* Corresponding author. Tel.: +1 418 545 5011 ext. 5057; fax: +1 418 545 5012.
E-mail address: andre_charette@uqac.ca (A. Charette).
URLs: http://www.uqac.ca/recherche/unites/grips.html, http://www.uqac.ca/recherche/unites/cural.html.

1290-0729/$ – see front matter
doi:10.1016/j.ijthermalsci.2005.09.007

Nomenclature

C	light velocity	$\mathrm{m\cdot s^{-1}}$
$\frac{d}{d}$	implicit differentiation	
ES	emerging signals	$\mathrm{W\cdot m^{-2}}$
f	scattering phase function	
g	anisotropy factor	
I	directional intensity	$\mathrm{W\cdot m^{-2}\cdot sr^{-1}}$
M	number of quadrature directions	
n	refractive index	
$\vec{n}$	outgoing normal to surface	
R	reflectance	$\mathrm{W\cdot m^{-2}}$
$\vec{r}$	position vector	m
S	energy source term	$\mathrm{W\cdot m^{-3}\cdot sr^{-1}}$
T	transmittance	$\mathrm{W\cdot m^{-2}}$
t	time	s

Greek symbols

β	extinction coefficient	$\mathrm{m^{-1}}$
Δx	mesh size	m
κ	absorption coefficient	$\mathrm{m^{-1}}$
ξ	direction cosine	
σ	scattering coefficient	$\mathrm{m^{-1}}$
Φ	fluence	$\mathrm{W\cdot m^{-2}}$
ω	quadrature weight	sr
$\vec{\Omega}$	directional vector	
$\mathrm{d}\Omega$	infinitesimal solid angle	sr
$\nabla\cdot$	divergence operator	$\mathrm{m^{-1}}$

Superscripts

c	collimated variables
n	time step
o	initial laser strength
$'$	incident direction
$*$	non-dimensional variable

Subscripts

b	boundary
i_{xj}	position j-coordinate subscript for $j:1\rightarrow n_{\mathrm{dim}}$
$i_{\vec{\Omega}}$	quadrature subscript
k	directional subscript

that, after few millimeters of travel, an incident beam is completely scattered. To mitigate scattering effects, longer wavelengths are preferable; nevertheless, to prevent absorption, the wavelengths window is essentially dependent on water and blood haemoglobin specific absorptions. Hence, near infra-red light, between 600 nm and 900 nm is utilized in optical tomography. However, the optical thickness, being essentially attributed to scattering as in biomedical imaging, prevents probing media of large dimensions. In this case, most of the emerging photons at a boundary measurement point have not followed a straight trajectory and do not come from the co-axially aligned collimated laser source on the other side of the material so that no back-projection method as the Radon transform can be used.

To improve imaging performance, a broad range of methods has been proposed. In the case of direct imaging, efforts have been put in isolating an un-scattered or least scattered component of the transmitted scattered light. This set-up explains the growing field of interest for the pulsed lasers. Transient laser impingement authorizes the detection of the earliest photons, thanks to time-gating techniques, assumed to be unscattered or to have undergone limited scattering [10,11]. Time-of-flight systems using a pulsed laser as a light source and time-resolved detectors allow the boundary measurement of the temporal intensity response function with a resolution of a few picoseconds [12]. Time-gating techniques may further be improved by an optical filtering of the emerging transmitted light in order to collect the collimated fraction of the earliest photons [13]. The underlying principle of these techniques is to separate the photons which have followed a straight line in order to apply on them back-projection methods. The merits of direct imaging is the recovery of internal structure with the use of relatively simple theoretical and numerical techniques, while inverse imaging necessitates a complete field of measurements and a numerical definition of the problem (geometry, boundaries, meshing and light transport model) in order to allow the implementation of an inverse algorithm [4,5]. However as stated above, direct imaging is limited by the intense scattering in the thickness of the material, while inverse problems are able to take advantage of this by accessing the information embedded in the diffuse photons; it provides only structural images and needs to work only in straight transmission. Not being able to allow a quantitative identification of the optical properties is an intrinsic limitation of the method. However, this non-intrusive safe and easily implemented method could benefit considerably from investigations on the effect of optical parameters on reflection and transmission behaviours. This is the object of the present paper.

Using information embedded in the temporal persisting signature due to scattering can allow overcoming the limitation on the optical thickness. First, as unscattered photons are not necessary, optical thickness becomes less important except in the case of preponderant absorption. Second, back-scattered photons may be used, leading to a more convenient device. The long term emerging photons have undergone multiple scattering events and visited deep areas in the medium. They provide a lot of information on the inside optical properties distribution. Theoretical investigations have opened the way of exploiting the asymptotic logarithmic slope (ALS) of the decaying part of the transient signature in reflectance or transmittance [14–16] for homogeneous material characterization. By fitting time-resolved measurements against solutions obtained from the diffusion approximation for Dirac-pulse light transport in turbid 1-D media, importance of the time-decaying log-slope of emerging reflected and transmitted signals for the retrieval of optical properties has been confirmed. In case of a layered material, it has been experimentally and numerically demonstrated [17] that the logarithm of the long-term reflected signal

is directly linked to the absorption coefficient of the deep layer when a (or several) superficial layer exists with a higher level of absorption. The effect of the latter is related only to the magnitude of the collected signal, not to the asymptotic log-slope. It thus appears that a direct imaging technique which could make use of the diffuse photons, which is not feasible with current remote probing set-up, would be an interesting technology.

In the following, it is intended to make a numerical exploration of the transient signature response, both in reflection and transmission, to the presence of an heterogeneity in a mono-dimensional domain. Furthermore, given some observations on a 1-D slab containing an heterogeneous layer, a probing procedure based on long term back-scattered photons is demonstrated on simple numerical phantoms in order to address the feasibility of direct local reflectance imaging of tissues using short laser pulses. First, the solution model for the transient radiative transfer equation (RTE) in a non-homogeneous medium is described. Second, a parametrical study in the case of 1-D homogeneous and non-homogeneous slabs is presented with the objective of providing a detailed description of the obtainable signals in reflection and transmission on a simple system. In a third part, direct imaging of 2-D non-homogeneous phantoms using reflected signals is explored.

Remark. In [4,5], complete reconstruction methods have been proposed, which use the precise transient forward model, utilized here, as part of an inverse methodology. The present study explores another way of optical imaging which can lead to more convenient applications without the use of the difficult inverse reconstruction procedure. The practical utilization of the latter, despite its great potential, is not yet available due to remaining theoretical, numerical and set-up difficulties. The reader may consult Refs. [18] and [32] for the respective assets and drawbacks of the inverse reconstruction method with respect to direct imaging. The present paper actually develops a methodology to overcome some of the direct imaging limitations.

2. The model

This part deals with the presentation of the solution methods for ultra-short laser pulse interaction with a semi-transparent non-homogeneous medium. In the first place, the physical theoretical background of the model is presented and then the numerical treatment is introduced.

2.1. Fundamentals

In order to treat the full hyperbolic nature of light pulse propagation in a semi-transparent medium, the time-dependent Boltzmann-type RTE given below [18,19] is used:

$$\frac{1}{C}\frac{\partial I(\vec{r},t,\vec{\Omega})}{\partial t}+\nabla\cdot\left(\vec{\Omega}\cdot I(\vec{r},t,\vec{\Omega})\right)+(\kappa+\sigma)I(\vec{r},t,\vec{\Omega}) = \overbrace{\frac{\sigma}{4\pi}\int_{4\pi} f(\vec{\Omega}',\vec{\Omega})I(\vec{r},t,\vec{\Omega}')\,\mathrm{d}\Omega'}^{(\mathbf{I})} \tag{1}$$

This equation describes the change in intensity $I(\vec{r},t,\vec{\Omega})$ of a light ray at a position $\vec{r}$ and time t in direction $\vec{\Omega}$ throughout its propagation at the light velocity C in the medium (constant refractive index different from unity), accounting for extinction sink term $(\kappa+\sigma)I(\vec{r},t,\vec{\Omega})$ due to absorption (κ) and out-scattering (σ), both in m^{-1}, properties which can be spatially variable in the non-homogeneous case. The source term present in the integral (I) addresses the redistribution of intensity due to in-scattering: the scattering phase function $f(\vec{\Omega}',\vec{\Omega})$ characterizes the intensity of a wave incident in direction $\vec{\Omega}'$ scattered in direction $\vec{\Omega}$. This formalism is essentially monochromatic. I is expressed in $\mathrm{W\cdot m^{-2}\cdot sr^{-1}}$. The development to the first order of the Henyey–Greenstein function is utilized (for the choice on the Henyey–Greenstein function, the reader is reported to [20]):

$$f(\vec{\Omega}',\vec{\Omega})=1+3g\cos(\vec{\Omega}',\vec{\Omega}) \tag{2}$$

where g is called the anisotropy factor and is in fact the mean cosine of the angles between the scattered direction $(\vec{\Omega})$ and the incident one $(\vec{\Omega}')$. In this condition, g cannot exceed an absolute value of 0.3, otherwise the validity of the Henyey–Greenstein function linearization would be jeopardized. Hence, isotropically $(g=0)$ and anisotropically $(g\neq 0)$ scattering events can be achieved.

Since physically no light exists in the medium before irradiation, the following initial condition is enforced:

$$I(\vec{r},0,\vec{\Omega})=0$$

The boundary conditions are defined as transparent and non-reflecting. The emerging signals (*ES*) as transmittance and reflectance are then computed in time by:

$$ES=\int_{\cos(\vec{\Omega},\vec{n})>0} I(\vec{r}_b,t,\vec{\Omega})\cos(\vec{\Omega},\vec{n})\,\mathrm{d}\Omega \tag{3}$$

This is the sum of the projected intensities I on the normal outward direction $\vec{n}$ to a boundary surface located around the position identified by $\vec{r}_b$. This formulation is required to predict hemispherical detector readings.

2.1.1. Collimated irradiation

Energy is injected in the system through incident pulse irradiation. Direction of this collimated beam is rectilinear and, in case of a pulse, its shape is transported at the velocity of light in the medium. Along its path, it undergoes extinction. Energy lost by the beam is gained by the medium through absorption and injected in the field of induced radiation intensity through scattering. Therefore, since Eq. (1) is governing the induced in-scattered radiation field, a source term coupling the collimated energy injection from the pulse is to be added:

$$S(\vec{r},t,\vec{\Omega})=\frac{\sigma}{4\pi}I^c\left(\vec{r},t,\vec{\Omega}^c\right)f\left(\vec{\Omega}^c,\vec{\Omega}\right) \tag{4}$$

where $\vec{\Omega}^c$ is the direction of the collimated irradiation $I^c(\vec{r},t,\vec{\Omega}^c)$ which is governed by Bouguer–Beer–Lambert extinction law:

$$\frac{1}{C}\frac{\partial I^c(\vec{r},t,\vec{\Omega}^c)}{\partial t}+\nabla\cdot\left(\vec{\Omega}^c\cdot I^c\left(\vec{r},t,\vec{\Omega}^c\right)\right)+(\kappa+\sigma)I^c\left(\vec{r},t,\vec{\Omega}^c\right)=0 \tag{5}$$

A collimated radiation wave travels at velocity C, following a direction given by $\vec{\Omega}^c$, which forms in fact a characteristics set. Along this spatio-temporal characteristic line, Eq. (5) becomes an ordinary differential equation which is integrated in a Lagrangian way, on a discretized domain, using a third order Runge–Kutta scheme [20–22] yielding a semi-analytical solution of the extinction adapted to fully non-homogeneous materials. The advantage of this separate treatment is twofold: the transport of the incident pulse without the use of a transport differential scheme which may lead to spurious diffusion or dispersion if the profile of the pulse is not smooth enough, and the use of an exact collimated direction which may not be matched, in the general case, by a direction of quadrature of the discrete ordinates model. Similar treatments of boundary emanating radiations have already been introduced for the homogeneous case [23–25].

Hence, boundary measurements (Eq. (3)) become:

$$ES = \int_{\cos(\vec{\Omega},\vec{n})>0} I(\vec{r}_b,t,\vec{\Omega})\cos(\vec{\Omega},\vec{n}) + I^c\big(\vec{r}_b,t,\vec{\Omega}^c\big)\cos\big(\vec{\Omega}^c,\vec{n}\big)H\big(\cos\big(\vec{\Omega}^c,\vec{n}\big)\big)\,\mathrm{d}\Omega \tag{6}$$

where H is the Heaviside function, equaling unity if its argument is positive and being null otherwise. The presence of this function allows the computation of the collimated beam in the emerging signal in the transmitted case only.

2.2. Numerical treatment

A powerful method to compute the multi-directional equation of radiative transfer is the so-called discrete ordinates method. The RTE (Eq. (1)) is solved on a discrete set of M spatial directions covering 4π sr solid angle, $(\vec{\Omega}_{i_{\vec{\Omega}}})_{i_{\vec{\Omega}}:1\to M}$, weighted so that space symmetry and boundary radiative balances are achieved. Each direction of quadrature is taken into account in order to compute the coupling scattering integral source term I (Eq. (1)) between all directional intensities (each directional intensity at each point of the domain gets a scattered fraction of all directional intensities—integrated over the whole space through the quadrature formula—at that point). The discrete ordinates method has to be coupled with numerical schemes for divergence calculation and time stepping [26]. In the following, the finite-difference method is used with, as numerical scheme, the *piecewise parabolic advection* (PPA) TVD scheme [27] already introduced for the numerical treatment of the RTE [28–30].

The discretized equation for the induced intensity field can be cast into the following form, intuitively based on Eq. (1):

$$\begin{aligned} I^{n+1}_{i_{x_j},i_{\vec{\Omega}}} &= I^n_{i_{x_j},i_{\vec{\Omega}}} - \sum_{k=1}^{n_{\mathrm{dim}}} \xi_{k,i_{\vec{\Omega}}} \frac{\Delta t C}{\Delta x_j}\big[I^n_{i_{x_j}+1/2k,i_{\vec{\Omega}}} - I^n_{i_{x_j}-1/2k,i_{\vec{\Omega}}}\big] \\ &\quad - \Delta t C(\sigma_{i_{x_j}} + \kappa_{i_{x_j}}) I^{n+1}_{i_{x_j},i_{\vec{\Omega}}} \\ &\quad + \Delta t C \frac{\sigma}{4\pi} \sum_{j_{\vec{\Omega}}}^{M} \omega_{j_{\vec{\Omega}}} f(j_{\vec{\Omega}},i_{\vec{\Omega}}) I^{n+1}_{i_{x_j},j_{\vec{\Omega}}} + S^{n+1}_{i_{x_j},i_{\vec{\Omega}}} \Delta t C \\ i_{\vec{\Omega}} &: 1 \to M \end{aligned} \tag{7}$$

Subscripts i_{xj} and $i_{\vec{\Omega}}$ are for spatial indexation/position in $j = 1, 2$ or 3 $(= n_{\mathrm{dim}})$ dimensions and $\vec{\Omega}$ direction, respectively. Superscripts $n+1$ and n give the corresponding time step. $I^n_{ixj+1/2k}$ and $I^n_{ixj-1/2k}$ are interpolated interfacial values at boundaries of the control volume centred in $(i_{x_j})_{j:1\to n_{\mathrm{dim}}}$ in direction k of derivation and are given by PPA formulations. $\xi_{k,i_{\vec{\Omega}}}$ is the k-direction cosine of quadrature $\vec{\Omega}$ while $\omega_{i_{\vec{\Omega}}}$ is the weight associated to it. $S^{n+1}_{i_{x_j},i_{\vec{\Omega}}} = \sigma_{i_{x_j}}/4\pi\, I^{c^{n+1}}_{i_{x_j}} f(\vec{\Omega}^c, i_{\vec{\Omega}})$ stands for the coupling source from Eq. (4).

Courant–Friedrich–Levy (CFL) number $(= C\Delta t/\Delta x)$ is set to unity for both induced and collimated intensity fields. Δt is the time step and Δx the spatial step. Grid is completely regular. However, in multi-D cases, CFL number must be reduced by half to ensure stability of the scheme for the treatment of the induced radiation field. To keep time synchronization between induced and collimated intensity solvers, two half-time steps are then defined for the induced intensity calculation so that the complete time step, sum of both half-time steps in the same iteration, corresponds to the same unity CFL number in both solvers. The integral in-scattering term (I) in Eq. (1) is solved iteratively within each half-time step because of implicit treatment. Eq. (7) is computed without the coupling collimated source $S^{n+1}_{i_{x_j},i_{\vec{\Omega}}}$ during the first half-time step to prevent some early photons to progress spuriously ahead of the collimated irradiation. The first half-time step is thus used for the stabilization of the numerical scheme and the total amount of energy from the collimated beam during the whole time step is injected in the second half-time step. However, this numerical procedure in multi-D configurations does not completely prevent anticipated progression of photons. Those are classical advection schemes drawbacks.

3. Mono-dimensional simulations

The aim of this parametrical study is to illustrate the behaviour laws of the transmitted and reflected signals with respect to the optical properties (absorption and scattering) distributions in a mono-dimensional slab. More specifically, the effect of an inclusion layer in a homogeneous slab on the remanent signature of the emerging reflectance and transmittance is analysed.

3.1. Physical model

The 1-D medium is assumed absorbing and scattering but non-emitting. It is constituted by three layers with different optical properties and thicknesses, except in the homogeneous case. Both external layers have always the same optical properties in order to mimic the background medium. The boundary surfaces are assumed non-reflecting and transparent. The upper one is irradiated by a collimated square laser pulse. Fig. 1 provides the configuration sketch.

3.2. Computation parameters

The following parameters have been retained for the numerical simulations of the 1-D slab:

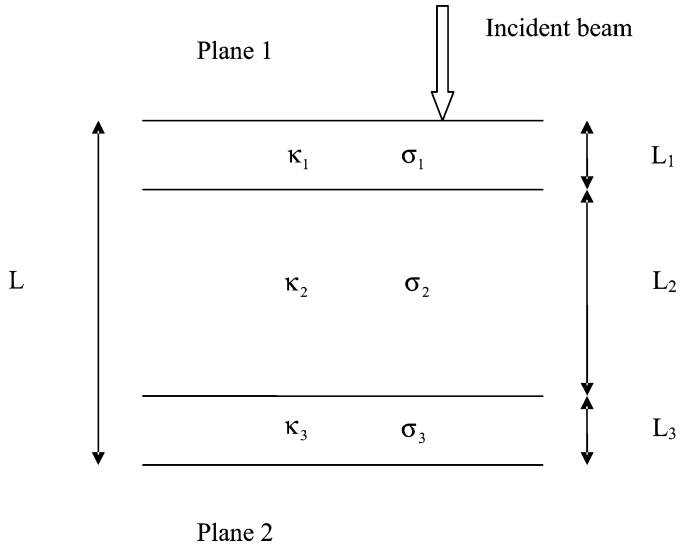

Fig. 1. Physical model.

- S_{12} quadrature;
- Normalised laser incident intensity I^o, from which dimensionless reflectance and transmittance are defined: $R^* = R/I^o$ and $T^* = T/I^o$, respectively. This choice of presentation of the results is different from what is seen for experimental work. This is explained by the difficulty in quantifying the coupling between the devices in which light is transported in the experiment. Hence, experimental curves for transmittance or reflectance are presented as self-normalized. In a numerical work, these constraints do not appear. It has to be noticed that, whatever the normalization, the temporal shape and, thus, the log-slope are not altered;
- The total slab thickness is 5×10^{-3} m;
- The refractive index is $n = 1.33$;
- Number of cells is 100;
- Number of time steps is between 1500 and 15000 in order to capture the long term signal behaviour;
- The nature of the scattering (forward, isotropic or backward) is the same in the whole slab;
- The laser pulse duration t_p defines the non-dimensional time $t^* = t/t_p$.

3.3. Results

3.3.1. Homogeneous slab

This section analyses the signals obtained in transmission and reflexion for a 1-D homogeneous slab exposed to an irradiated laser pulse. The laser pulse width is set at $t_p = 4.436$ ps. By varying the optical thickness (or the extinction coefficient $\beta = \kappa + \sigma$) within the material as well as the albedo magnitude ω, four families of optical signatures are observed which seem to give a generic classification of the different signatures for this optical system. Figs. 2 and 3 provide the diagram of classification for reflectance and transmittance in terms of extinction coefficient and albedo magnitudes. The scattering is isotropic.

The first family is presented in Figs. 2(a) and 3(a) and is linked to weak extinction ($\beta = 200$ m^{-1}) and large albedo ($\omega = 0.998$) within the medium. Physically, it means that the absorption is very weak. The transmitted pulse is recovered at the emergence face (Fig. 2(a)). The second family, Figs. 2(b) and 3(b), is defined by large extinction ($\beta = 2000$ m^{-1}) and albedo ($\omega = 0.998$), which results in a relatively weak absorption but a high scattering coefficient. Since scattering is predominant and redistributes the energy lost by the initial pulse in the whole intensity field, the signal is spread in time and the pulse has disappeared in the transmittance signature (Fig. 2(b)). Reflectance, which depends only on the scattering strength, is logically larger, Fig. 3(b). The third family (Figs. 2(c) and 3(c)) corresponds to a medium with weak albedo ($\omega = 0.2$) and extinction ($\beta = 200$ m^{-1}). Then, the transmitted pulse is almost unchanged (Fig. 2(c)) because it is not attenuated and the small energy lost by the collimated beam is absorbed by the medium and not kept by scattering in the whole intensity field. Consequently, reflectance is small, Fig. 3(c). The last family (Figs. 2(d) and 3(d)) deals with weak albedo ($\omega = 0.2$) but a high extinction coefficient ($\beta = 2000$ m^{-1}). Hence, high absorption and relatively weak scattering are expected. The transmitted pulse is thus attenuated, Fig. 2(d), and only a small fraction of the attenuated energy is recuperated by scattering. This yields a moderate level of reflectance, Fig. 3(d).

As seen, the signals are well characterized by two parameters: the extinction coefficient β and the albedo ω of the medium. The extinction coefficient β determines the transmitted pulse attenuation. If the albedo ω is weak, a small portion of the attenuated energy is recuperated by scattering (extinction is mainly due to absorption) and the shape of the pulse is basically conserved, regardless of the transmission magnitude. When the albedo is high, the scattering events which lead to the attenuation of the transmitted pulse redistribute the energy in time, creating a persistent signature. Concerning the reflected signals, as they depend only on scattering, their magnitude is dependent on a combination of β and ω, like the product $\beta\omega$ (equalling the scattering strength itself) for instance. The signal duration is not favoured by a small albedo.

The nature of scattering is not expected to modify those qualitative behaviours, as found in Figs. 4(a) and 4(b). With backward scattering, the transmittance signature is stretched in time and its maximum value decreases when compared to isotropic scattering, Fig. 4(a). Forward scattering exhibits an opposite behaviour. As expected, the reflectance maximum increases for backward scattering, Fig. 4(b).

3.3.2. Heterogeneous slab

The slab is now considered non-homogeneous, with its internal layer (see Fig. 5) optical properties different from those of the external layers (background medium). The position and thickness of the inclusion layer are allowed to vary as well.

General characteristics. It is intended to discuss the opportunity of having an ultra-short pulse in order to probe an heterogeneous system. The inherent problem of ultra-short laser pulses is the small injected energy which prevents probing large mate-

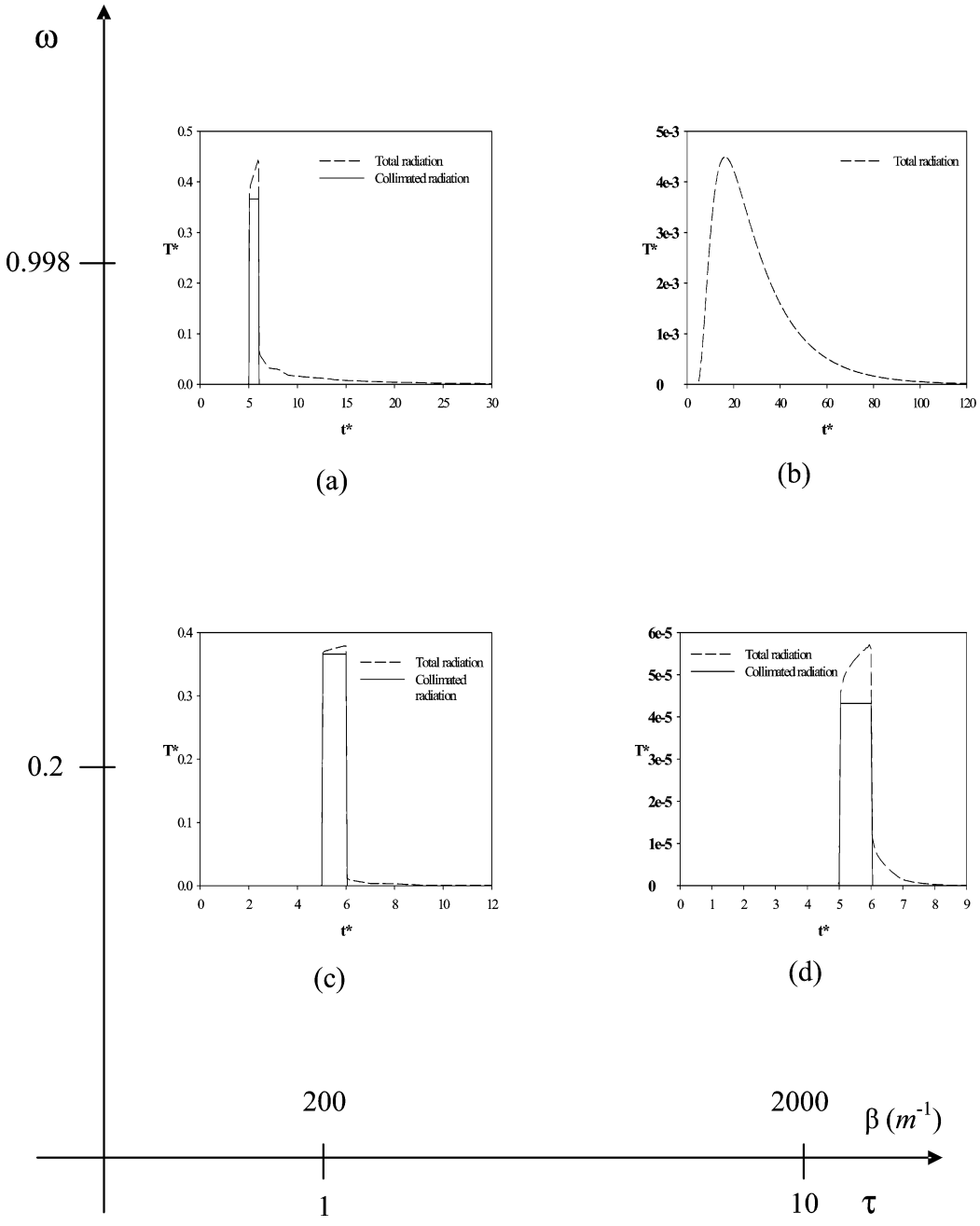

Fig. 2. Representation of family of signals in transmission, pulse width equal to 4.436 ps, isotropic scattering.

rials with a high signal to noise ratio. Figs. 6 and 7 give some interesting information about the choice of the laser pulse width. In Fig. 6, a short pulse is used ($t_p = 1$ ps) and transmittance (picture (a)) and reflectance (picture (b)) are shown as function of time for different positions of the inclusion layer depicted in Fig. 5. The optical properties of the latter are $\kappa = 40\ \mathrm{m}^{-1}$ and $\sigma = 9000\ \mathrm{m}^{-1}$ and the slab background is set at $\kappa = 60\ \mathrm{m}^{-1}$ and $\sigma = 11000\ \mathrm{m}^{-1}$. It is seen that information about the presence and the position of the inclusion is provided by the asymptotic logarithmic decay, both in transmittance and reflectance. The asymptotic log slope (ALS) is ideally defined when the slope of the long term emerging signal logarithm becomes time-independent.

This feature will be further analysed in the next section. Fig. 7 displays similar graphs but, in this case, the incident laser pulse width is sufficiently long ($t_p = 1000$ ps) to have the reflectance and transmittance reach the steady regime (i.e., the level of the signal that would be kept if the laser would be continuous). Similarly, the information appears only in the decaying part of the signal. These results address the usual belief that ultra-short laser pulses are needed to gather the information about the optical parameters of the system embedded in the remanent time-dependent signature of the reflected or transmitted signals. It is shown here that the relevant part of this signature is the decaying one. Literature [14–17] reports results along this line about properties characterization of ho-

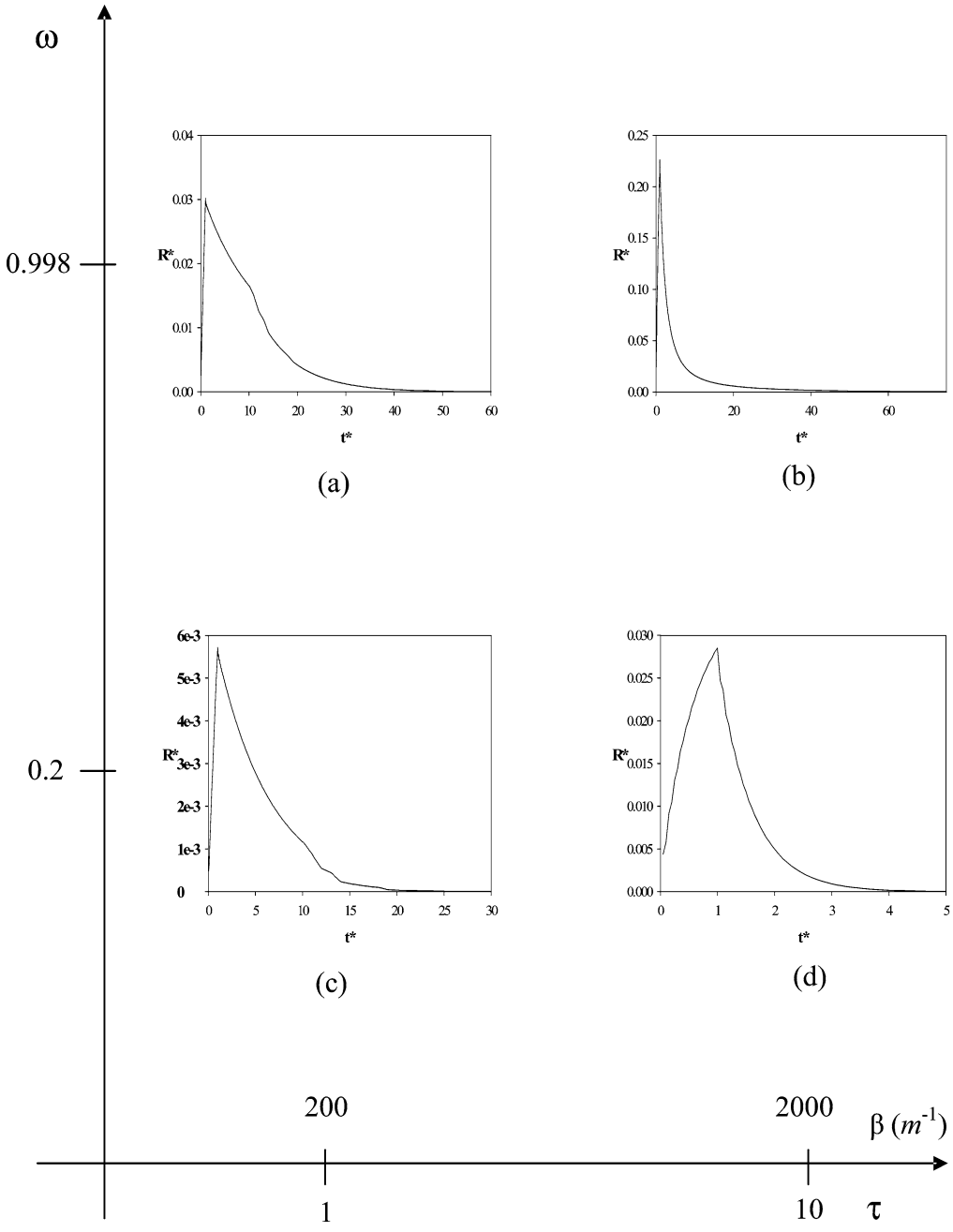

Fig. 3. Representation of family of signals in reflexion, pulse width equal to 4.436 ps, isotropic scattering.

mogeneous or layered media. However, in the case presented here, the information sought deals with the determination of the position of an embedded heterogeneous layer and not the optical properties of the material. Therefore, it is important to capture the decaying part of the signal after the pulse crosses the medium. The duration of the pulse is not critical in the present context. Obviously, other remote probing techniques as the ones based on the mean-time-of-flight of an emerging pulse are not concerned by this observation since, in that case, a sufficiently short pulse must be used [12]. Thus, it is worth using longer laser pulses in order to promote injection of energy in the system and focusing only on the signature decaying trend: by this way, the relevant information is obtained with an improved signal to noise ratio. Nevertheless, in order to avoid computational burden, the pulse width is kept here at: $t_p = 1$ ps.

A more extended parametrical study on the three layered slab is presented below. First, the effects of optical properties of the internal layer are investigated. By varying the scattering and absorption coefficients of the imbedded layer, modifications in the transmitted and reflected signatures are observed. Second, the geometrical thickness and position of the internal layer are given further attention. For easier comparisons, the extinction coefficient is set at a value of 1000 m^{-1} within the whole slab while the albedo of the background medium (both external layers) is prescribed at 0.7.

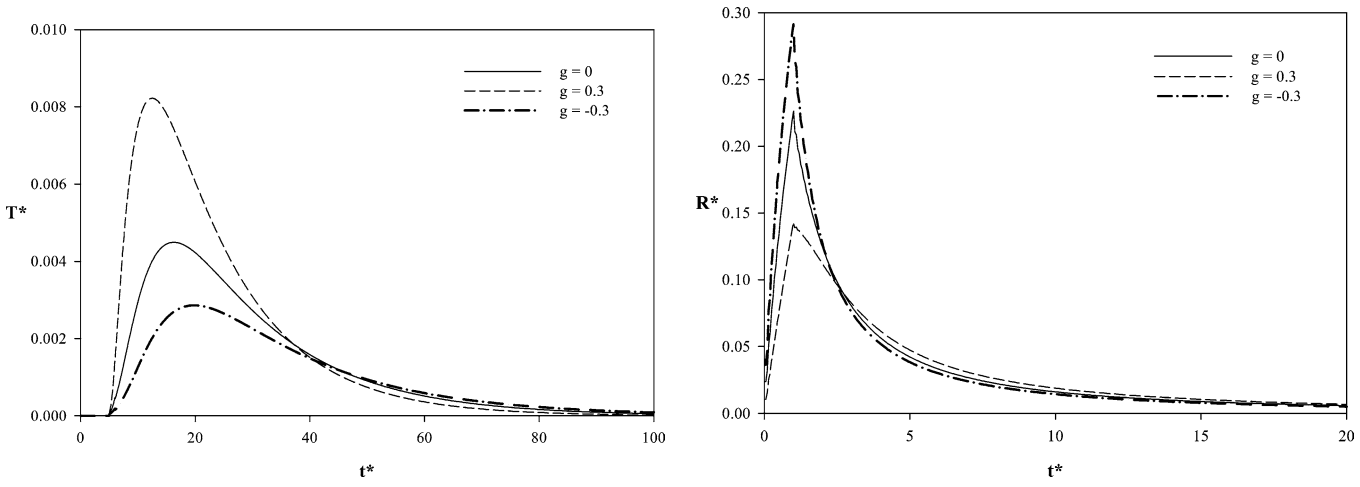

Fig. 4. Effect of the phase function on the transmittance (a) and the reflectance (b), respectively. Homogeneous case; $\omega = 0.998$; $\beta = 2000\ \mathrm{m}^{-1}$; $\tau = 10$.

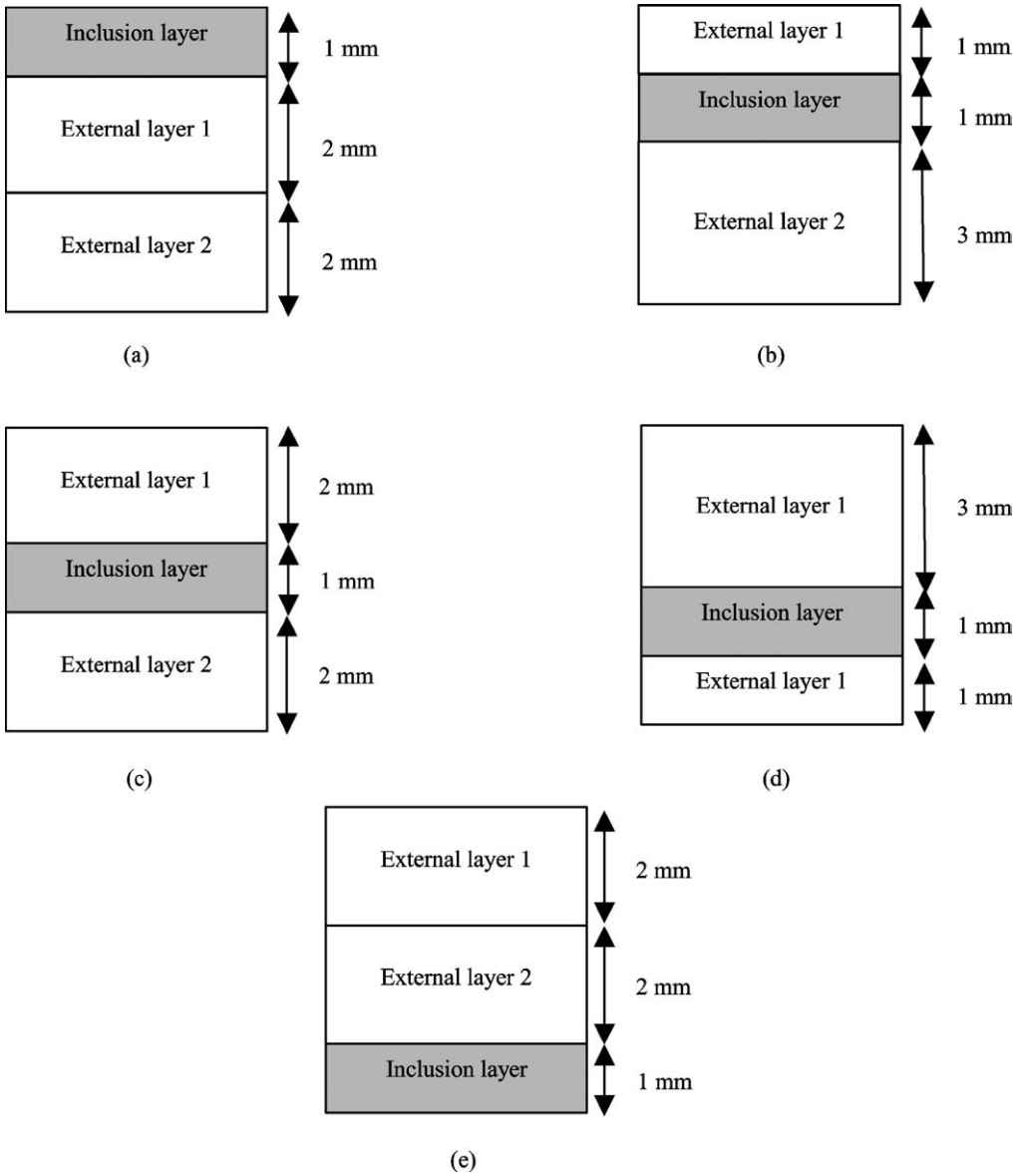

Fig. 5. Different positions of the inclusion layer. (a): Position 0. (b): Position 1. (c): Position 2. (d): Position 3. (e): Position 4.

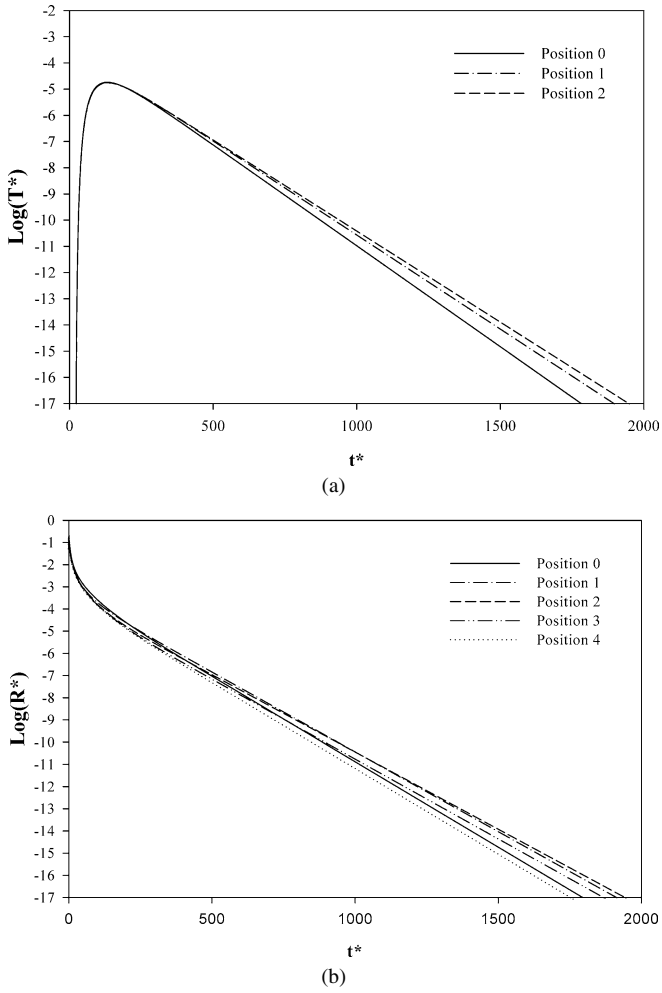

Fig. 6. Effect of different positions of the inclusion layer on the transmittance (a) and the reflectance (b), respectively. Pulse width equals to 1 ps.

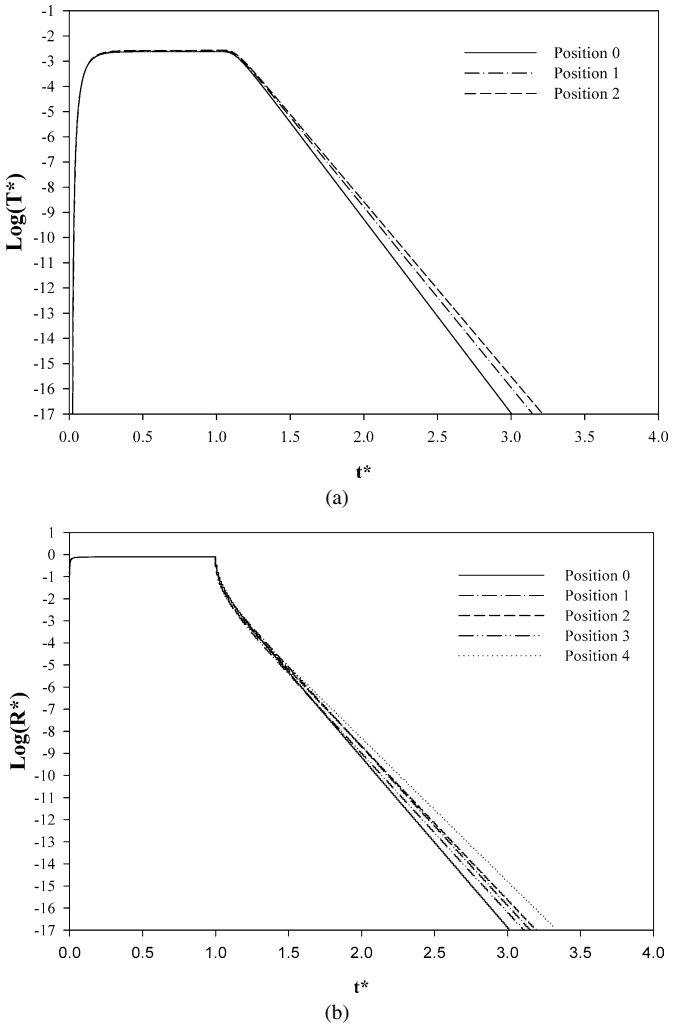

Fig. 7. Effect of different positions of the inclusion layer on the transmittance (a) and the reflectance (b), respectively. Pulse width equals to 1000 ps.

Effect of the internal layer scattering property. In this case, the thickness of the external layers is $L_1 = L_3 = 1$ mm.

Transmittance: When the scattering coefficient (isotropic case) increases in the internal layer (with a constant extinction coefficient $\beta = \sigma + \kappa$ within the material), the transmitted signal increases, Fig. 8(a). For large levels of scattering (albedo of the internal layer $\omega_2 = 0.998$, very close to unity), the transmittance signature persists long after the pulse has left the medium. This feature is due to photons retention induced by scattering. It can be concluded that an increase of the albedo of the internal layer brings about a higher level of the signal with time, and thus clearly indicates the presence of an heterogeneity.

In Fig. 9(a), it is seen that, for different types of scattering (backward, isotropic or forward), transmittance is divided in two parts. Note that a given type of scattering is prescribed within the whole slab. In the first part, $t^* < 90$, the transmittance magnitude is larger for forward scattering ($g = 0.3$), as expected, because the scattering events push the photons ahead so that they emerge sooner. For larger time ($t^* > 90$), the magnitude in the case of backward scattering ($g = -0.3$) becomes predominant. This is explained by the fact that, in case of backward scattering, photons are kept in the material and are expulsed very gradually in time. This phenomenon in the layered slab does not qualitatively differ from the one in the homogeneous case.

Reflectance: Fig. 8(b) for reflectance exhibits a similar trend as for transmittance, i.e. the reflectance increases when scattering increases in the internal layer. Reflectance is completely dependent on scattering. Thus, the larger the internal layer scattering is, the more reflectance is obtained. In Fig. 9(b), it is seen that the reflectance responses may be decomposed in three parts, with respect to the scattering type:

- for $t^* < 20$, the laser pulse has crossed the material. This may be observed by comparing with the transmittance, Fig. 9(a), where the transmitted pulse is clearly identified at early times and disappears around $t^* = 20$. Reflected signal is at its maximum here. It has significantly increased during the penetration of the pulse in the material and has been maintained at a high level thanks to back-scattered photons of the first generation (i.e. the photons which have been taken from the pulse and directly back-scattered). This

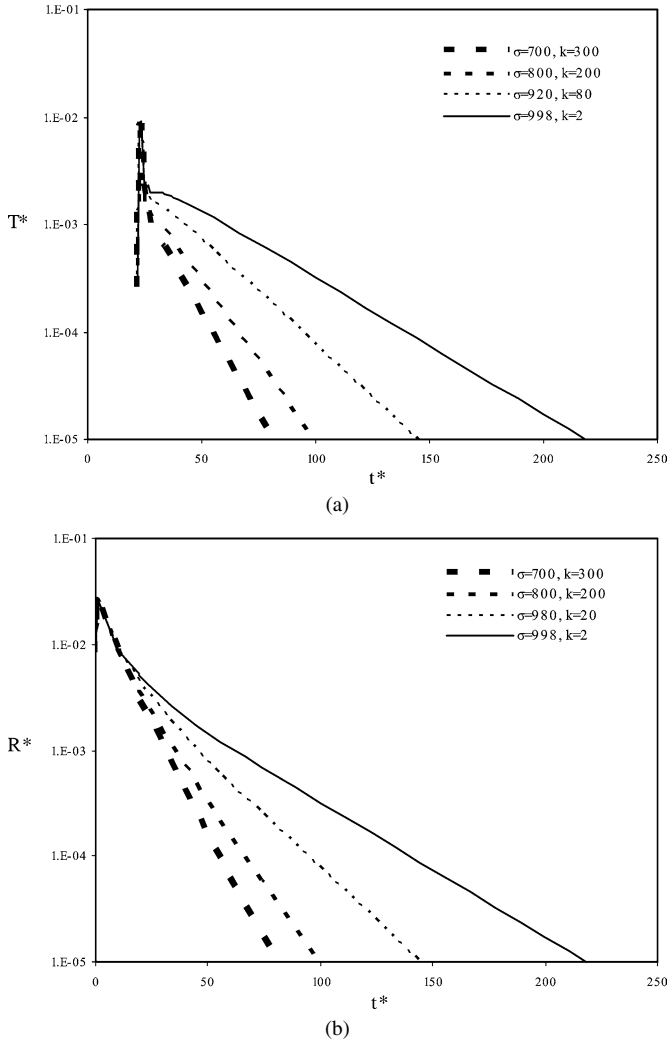

Fig. 8. Effect of the internal layer scattering coefficient on the transmittance (a) and the reflectance (b), respectively. Isotropic scattering case; $L_1 = L_3 = 1$ mm and $L_2 = 3$ mm; $\sigma_1 = \sigma_3 = 700\ \mathrm{m}^{-1}$ and $\kappa_1 = \kappa_3 = 300\ \mathrm{m}^{-1}$. In the graphs, σ and κ are the coefficients of the internal layer. The extinction coefficient $\beta = \sigma + \kappa$ is uniform at $1000\ \mathrm{m}^{-1}$ throughout the material.

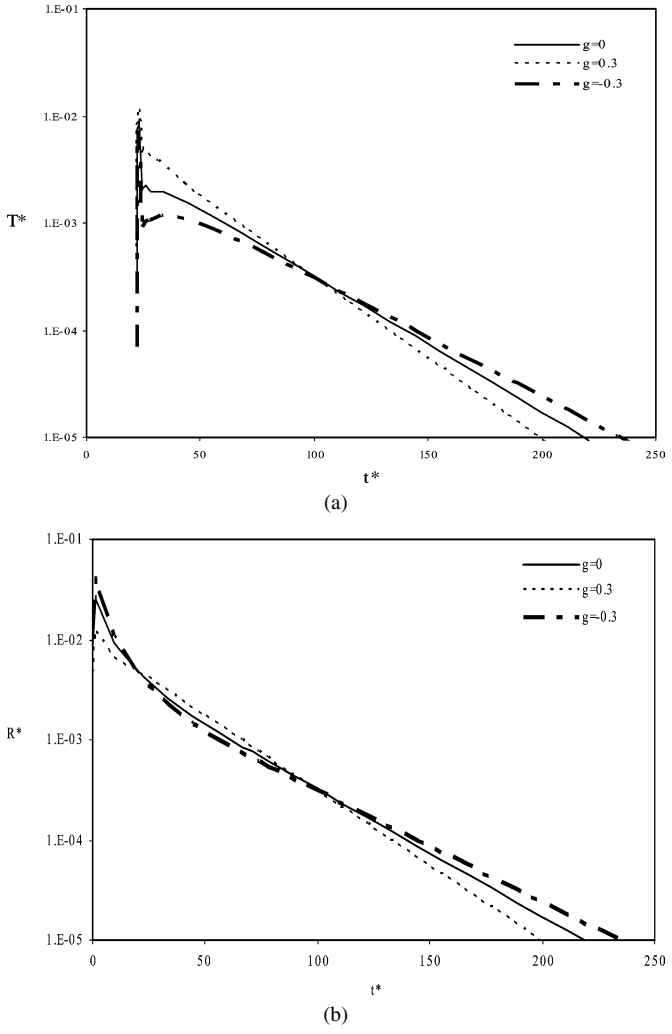

Fig. 9. Effect of the phase function on the transmittance (a) and the reflectance (b), respectively. $L_1 = L_3 = 1$ mm and $L_2 = 3$ mm; $\sigma_1 = \sigma_3 = 700\ \mathrm{m}^{-1}$ and $\kappa_1 = \kappa_3 = 300\ \mathrm{m}^{-1}$; $\sigma_2 = 998\ \mathrm{m}^{-1}$ and $\kappa_2 = 2\ \mathrm{m}^{-1}$. The same type of phase function is uniformly assigned to the whole slab.

explains why, in this part, reflected amplitude in case of backward scattering is the largest.

- $20 < t^* < 90$, the initial beam has just left the medium. In this time span, similarly to transmittance, forward scattering pushes many photons towards the boundaries, making the reflected signal larger for this type of scattering.
- $t^* > 90$, only the long lasting photons now emerge. They have been retained in the slab by backward scattering events. The medium is diffusively evacuating this residual light which back-scattering has retained for longer time for both transmittance and reflectance cases.

In summary, the same trends are found for the reflectance and transmittance behaviours. In one hand, the signal signature is sensitive to the scattering properties of the inclusion within the slab and, on the other hand, the behaviour, when the quality of scattering changes in the whole slab, is similar to the one observed in the homogeneous case.

Effect of stratification. The effects of the position and thickness of the internal layer are now studied in the case of a high scattering layer. In order to focus on theses effects, the optical properties are kept unchanged. The geometry of each layer (external or internal) is defined on each corresponding figure.

Figs. 10 and 11 show the transmitted and reflected responses to different stratifications of the 1-D slab. In Fig. 10, the internal layer is thickened towards the incident boundary while in Fig. 11 the thickening is towards the emerging boundary. It is noted that the amplitude of both transmittance and reflectance increases as the thickness of the internal layer increases, regardless of the direction of thickening. This can be explained by the fact that the more the central zone is thick, the more scattering is prevailing (for the same level of extinction), with a consequence that the energy recuperated in the form of transmittance and reflectance increases.

Fig. 12 provides explicit comparison of reflected and transmitted signals for two symmetrical stratifications and it is observed that the symmetry is partially recovered in the emerging signals. In Fig. 12(a), both transmittances are almost equal

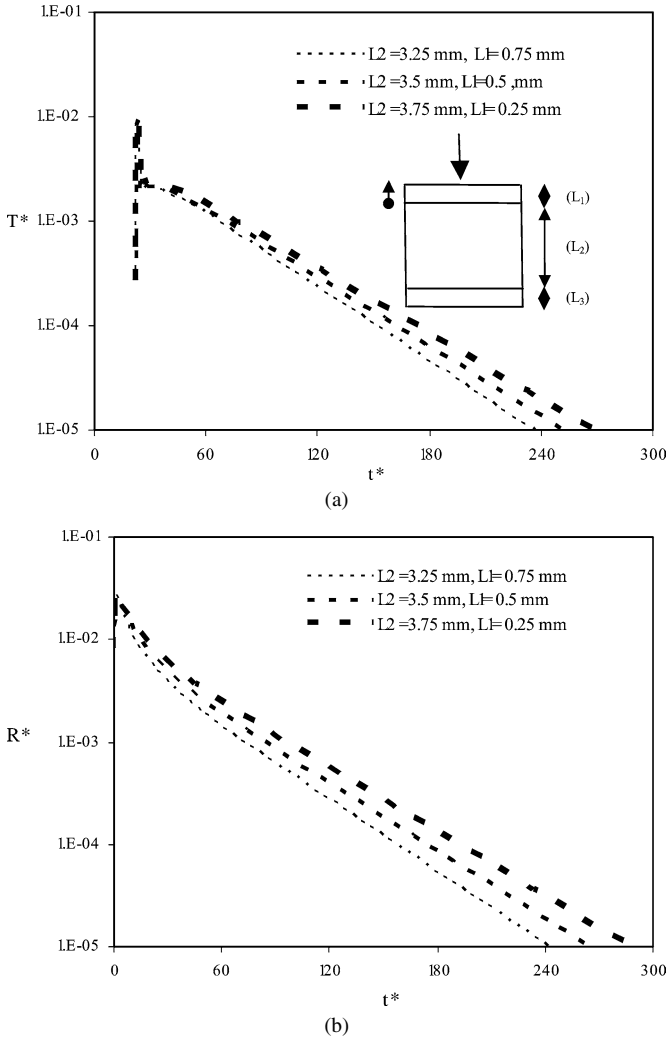

Fig. 10. Effect of layer thicknesses on the transmittance (a) and the reflectance (b), respectively. Isotropic scattering case; displacement towards incident layer; $L_3 = 1$ mm; $\sigma_1 = \sigma_3 = 700\ \mathrm{m}^{-1}$ and $\kappa_1 = \kappa_3 = 300\ \mathrm{m}^{-1}$; $\sigma_2 = 998\ \mathrm{m}^{-1}$ and $\kappa_2 = 2\ \mathrm{m}^{-1}$.

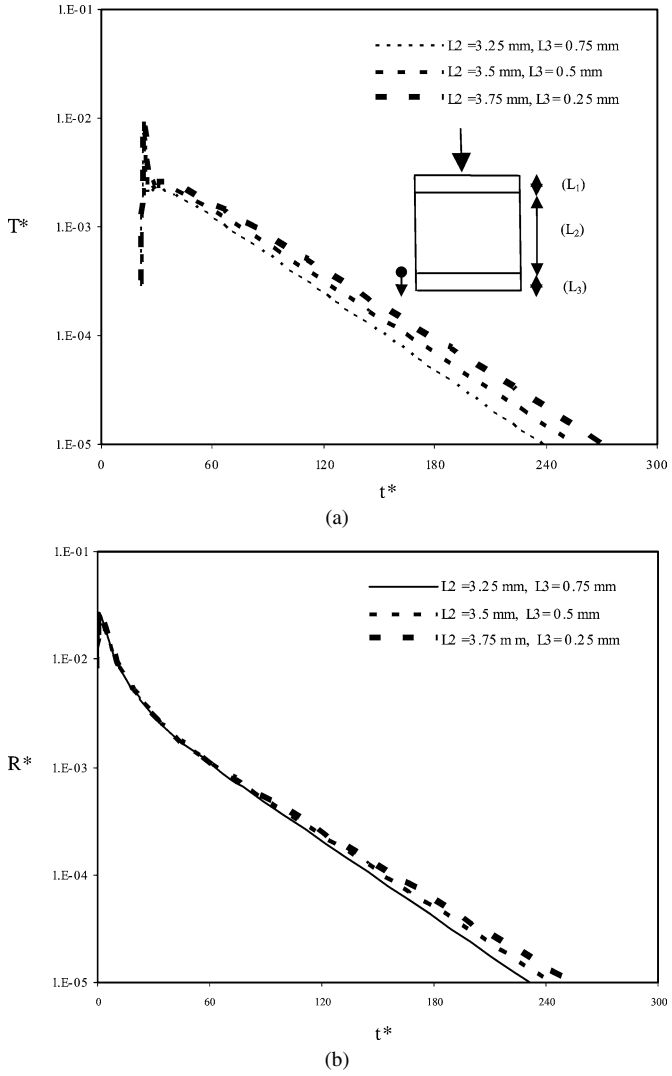

Fig. 11. Effect of layer thicknesses on the transmittance (a) and the reflectance (b), respectively. Isotropic scattering case; displacement towards emergent layer; $L_1 = 1$ mm. $\sigma_1 = \sigma_3 = 700\ \mathrm{m}^{-1}$ and $\kappa_1 = \kappa_3 = 300\ \mathrm{m}^{-1}$; $\sigma_2 = 998\ \mathrm{m}^{-1}$ and $\kappa_2 = 2\ \mathrm{m}^{-1}$.

while the reflected asymptotic log-slopes, Fig. 12(b), seem to be identical even if the absolute reflectances are not. This latter difference is explained by the fact that reflectance is not promoted when the scattering internal layer is in the farthest position from the incident boundary. For transmittance, the overall level of magnitude is less position-sensitive since in both symmetrical stratifications, the whole slab is visited by the photons. The effect of symmetry observed in Fig. 12 points out an interesting problem: the fact that detection may be unreliable in some cases where two different configurations may lead to the same slope.

3.4. Summary

Globally, the 1-D non-homogeneous case does not qualitatively differ from the homogeneous one. However, position and optical properties of the internal layer, viewed as an inclusion, strongly influence the time-dependent transmitted and reflected signals. It is particularly true for a high scattering inclusion with respect to the background medium optical properties. The major feature providing information about the internal stratification is found to be the asymptotic logarithmic slope of the reflectance and transmittance.

4. 2-D reconstruction

Based on the observations resulting from the 1-D slab, simulations are now carried out for the 2-D case with embedded heterogeneities. It was noted in the 1-D case that the presence of a heterogeneity layer implies a modification of the asymptotic logarithmic decaying in the reflected transient signature, depending on the position of this layer. It is similarly assumed in the following that the presence of an inclusion in a 2-D (or 3-D) medium in the line of sight of the probing laser beam leads to a modification of the logarithmic decay of the reflected transient signature at the point where the pulse is applied. Fig. 13 illustrates our purpose by showing the modification of the logarithmic slope of the back-scattered signal at the centre point of the boundary of a square medium for homogeneous and het-

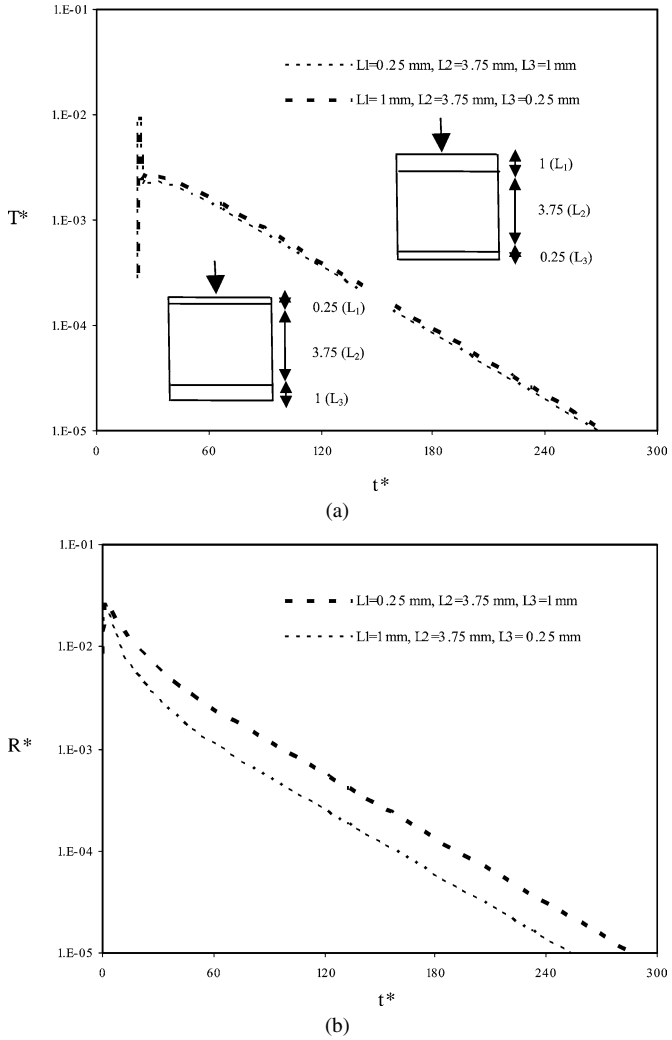

Fig. 12. Effect of displacement of internal layer on the transmittance (a) and the reflectance (b), respectively. Isotropic scattering case; $\sigma_1 = \sigma_3 = 700\ \mathrm{m}^{-1}$ and $\kappa_1 = \kappa_3 = 300\ \mathrm{m}^{-1}$; $\sigma_2 = 998\ \mathrm{m}^{-1}$ and $\kappa_2 = 2\ \mathrm{m}^{-1}$.

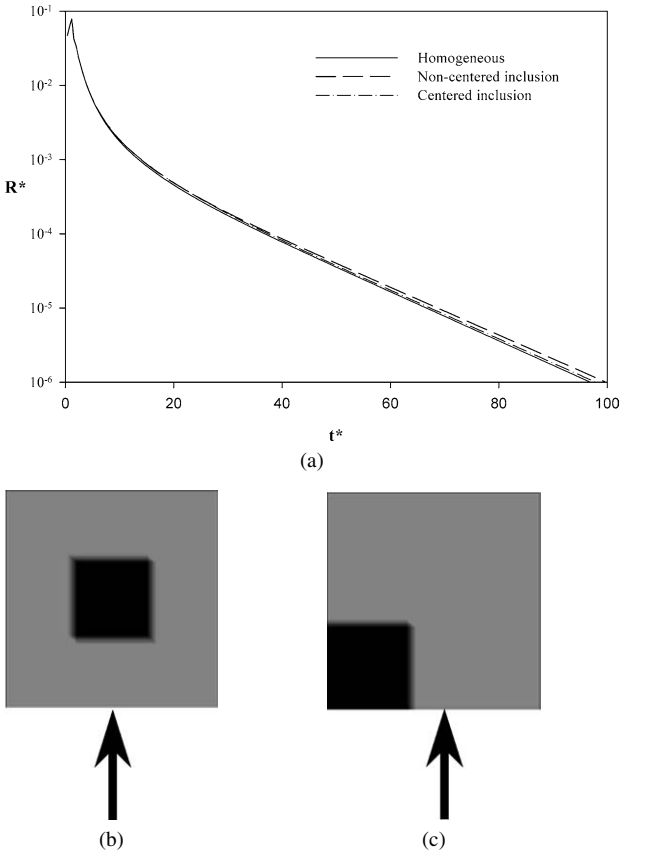

Fig. 13. (a): Reflectance signal R^* on a homogeneous and two heterogeneous square media. (b): Square phantom with a centered inclusion. (c): Square phantom with a non-centered inclusion. Absorption coefficient of the background (and of the homogeneous phantom) is 20 m^{-1} and scattering coefficient is 9980 m^{-1}, while absorption coefficient of the heterogeneity is 15 m^{-1} and scattering coefficient is 13000 m^{-1}. The arrow indicates the pulse impingement and the point of collection of the back-scattered photons for the homogeneous and non-homogeneous phantoms.

erogeneous phantoms with two positions of the heterogeneity. Clearly, it is observed that the asymptotic log-decay is perturbed by the non-homogeneity in the semi-transparent material. It seems difficult to link the log-slope to a particular feature of the heterogeneity (optical properties, position with respect to the measuring point), besides the fact that the presence of a lower absorption area in the medium (the heterogeneity) naturally leads to a globally higher level of reflectance and consequently to a weaker log-decay. The fact that the highest level of reflectance is not encountered for the case of the centred inclusion (picture (b)) shows how much the light trajectory is far from being a straight path, due to intense scattering. By back-projecting the local discrepancy in the log-slope along the line of sight at different probing positions around the medium, it is assumed that the location—but not the intrinsic nature—of a given heterogeneity may be identified. This allows the use of reflected signals for direct imaging, which represents a set-up improvement in applied cases, as explained in the introduction. As the probing is done on distances large compared to the spatial scales of the inclusion, it is assumed that the non-specificity demonstrated on Fig. 12 and which seems to be linked to a particular 1-D layering is not encountered here. It does not prevent however that other kinds of non-specificity exist.

The 2-D simulations were conducted with the following parameters. The mesh is 25×25 and the S_8 quadrature is used. A hundred pulses are shot around the square. Two hundred and fifty time steps are used in order to reach the log-asymptotic regime of the decaying reflected signal. The reference background medium coefficients are $\kappa = 20\ \mathrm{m}^{-1}$ for absorption and $\sigma = 9980\ \mathrm{m}^{-1}$ for scattering, leading to an optical thick medium of thickness $\tau = 10$ and albedo $\omega = 0.998$. Forward scattering is computed by using $g = 0.3$ in Eq. (2). The refractive index is $n = 1.33$ and the pulse duration is based on the mean free path time in the reference medium, $1/(\kappa + \sigma)C$, where C is the light velocity in the material. This time length is used in the non-dimensional time definition: $t^* = t \times (\kappa + \sigma)C$. The initial laser strength is I^o and it enters in the definition of all the normalized variables such as $R^* = R/I^o$, the non-dimensional reflectance. The asymptotic logarithmic slope is then defined as $\lim_{t^* \to \infty} \mathrm{d}(\log_{10} R^*)/\mathrm{d}t^*$. The optical properties of the heterogeneities are recalled in the figures and their respective captions when necessary.

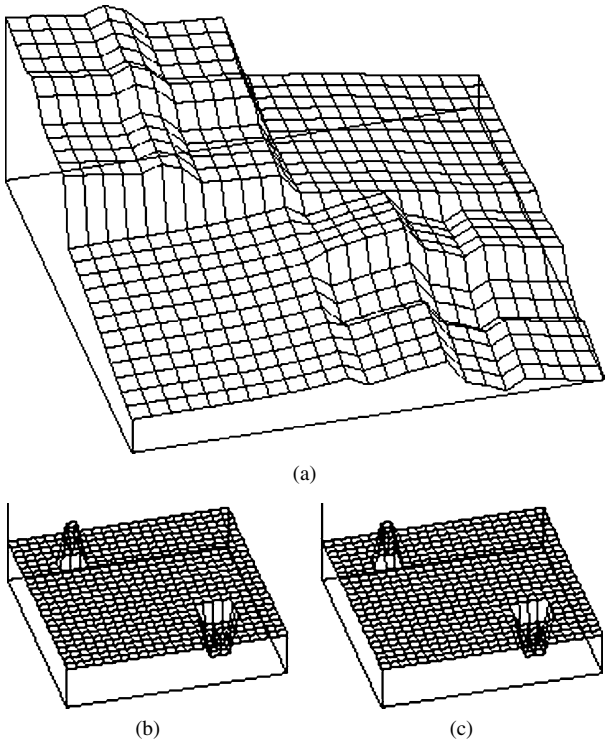

Fig. 14. (a): Reconstruction by back-projecting the relative log-slopes of reflected signals on a distance corresponding to the half dimension of the phantom. (b): Prescribed absorption coefficient field (up 25 m^{-1}, down 15 m^{-1}, background 20 m^{-1}). (c): Prescribed scattering coefficient field (up 13000 m^{-1}, down 7000 m^{-1}, background 9980 m^{-1}). Range of the relative log-slopes: 2.236×10^{-9}–2.417×10^{-9}.

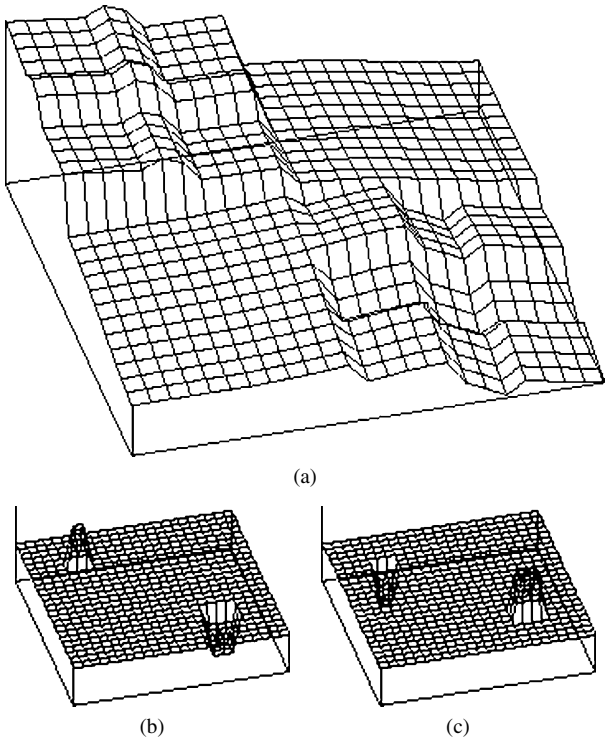

Fig. 15. (a): Reconstruction by back-projecting the relative log-slopes of reflected signals on a distance corresponding to the half dimension of the phantom. (b): Prescribed absorption coefficient field (up 25 m^{-1}, down 15 m^{-1}, background 20 m^{-1}). (c): Prescribed scattering coefficient field (up 13000 m^{-1}, down 7000 m^{-1}, background 9980 m^{-1}). Range of the relative log-slopes: 1.163×10^{-9}–1.272×10^{-9}.

Figs. 14–17 illustrate the process of reconstruction computed with a 2-D algorithm already described elsewhere [4]. A laser pulse is emitted at each node around the boundary and normal to it. The reflected signal is recorded and the long term logarithmic slope is applied along the half line of sight (relative to the dimension of the square) towards the interior of the material. At the beginning of the numerical experiment, the discretized domain is seen as a matrix with all coefficients equal to unity. Then, back-projecting the value of the log-slope is achieved by simply multiplying the coefficients of the matrix belonging to the corresponding half line of sight by the log-slope magnitude itself. Since several lines intersect each other (after a complete rotation of the laser probe around the square), each coefficient of the matrix has been multiplied twice at the end of the process, allowing a two-dimensional location of the heterogeneity in the depth of the material with the help of the distribution of this log-slopes combination (product). In this paper, qualitative log-slope product repartition has been retained for the demonstration of the feasibility of this new imaging procedure, but experiments would be necessary to ascertain the quantitative limits of use and the best investigation set-up for practical exploitation.

Several observations can already be made at the light of these first numerical results: (i) the location of the heterogeneities and their geometrical dimensions are well retrieved. The small order of magnitude of the reported log-slopes combination is due to the non-dimensionalization chosen (laser intensity for the reflected signal and pulse duration—equal to one mean free path time in the material—for time; see the last paragraph of this section) and should not induce a quantitative limitation of the method in practical applications. (ii) The nature of the heterogeneities (absorbing, scattering ...) seems not to be identifiable. For instance, on Figs. 14 and 15, pictures (a) and (b) may suggest to link the level of the local log-slopes combination to the level of contrast in absorption. However, Fig. 16 shows that this conclusion is wrong. As it can be observed in this figure, despite the fact that the level of absorption is high at the location of both heterogeneities, the corresponding local log-slopes combination level is lower than the one in the surrounding area (see arrows). Moreover, it is seen in Figs. 14–17 that the scattering property of a heterogeneity with respect to the background medium cannot be linked to a log-slope behaviour. For instance, in Figs. 14 and 15, the scattering nature of both heterogeneities is permuted (picture (c)) for the same absorption distribution (picture (b)) but the corresponding reconstruction (picture (a)) reflects in no way this inversion of the scattering configuration. It can be noted however that the overall range of the log-slopes product contributing to these reconstructions seems to account for the change in the scattering distribution since its order of magnitude is reduced by half from Fig. 14 (2.236×10^{-9}–2.417×10^{-9}) to Fig. 15 (1.163×10^{-9}–1.272×10^{-9}). All these observations tend to show that interactions exist between the heterogeneities present in the domain. The way an heterogeneity is localized

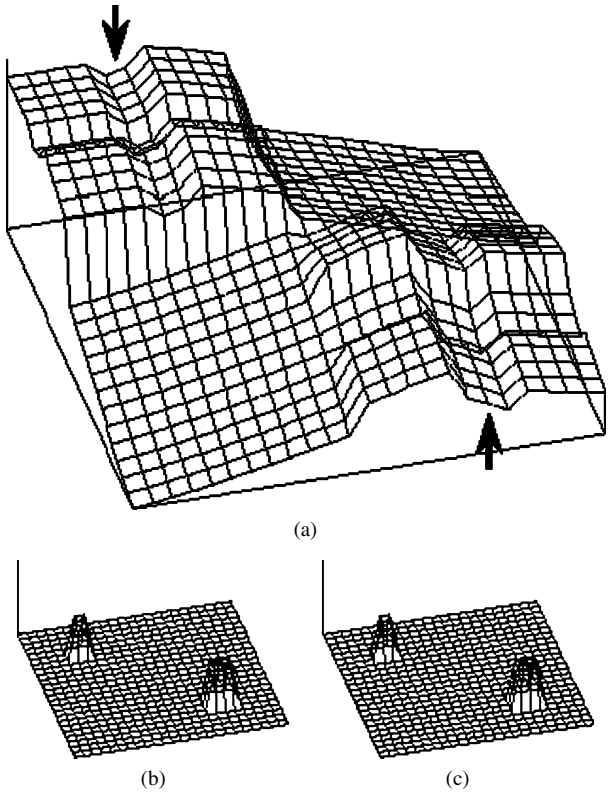

Fig. 16. (a): Reconstruction by back-projecting the relative log-slopes of reflected signals on a distance corresponding to the half dimension of the phantom. (b): Prescribed absorption coefficient field (up 25 m^{-1}, background 20 m^{-1}). (c): Prescribed scattering coefficient field (up 13000 m^{-1}, background 9980 m^{-1}). Range of the relative log-slopes: 1.004×10^{-8}–1.036×10^{-8}.

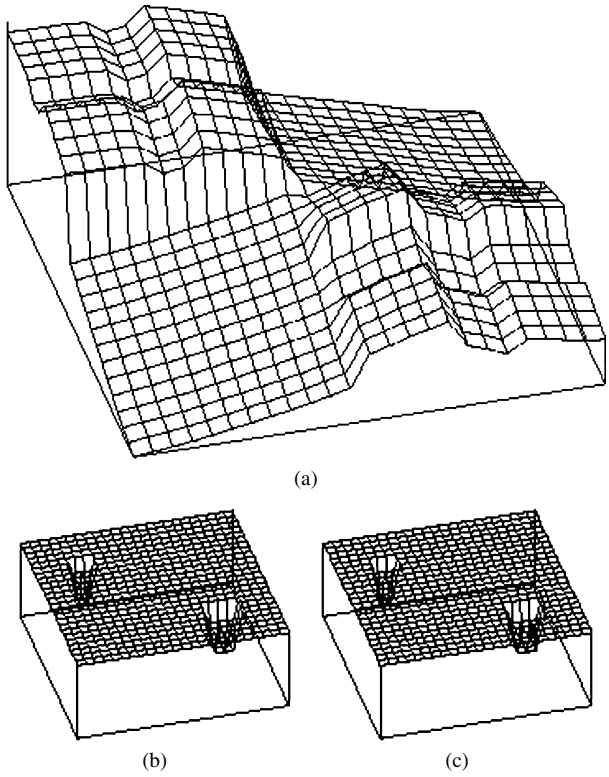

Fig. 17. (a): Reconstruction by back-projecting the relative log-slopes of reflected signals on a distance corresponding to the half dimension of the phantom. (b): Prescribed absorption coefficient field (down 15 m^{-1}, background 20 m^{-1}). (c): Prescribed scattering coefficient field (down 7000 m^{-1}, background 9980 m^{-1}). Range of the relative log-slopes: 1.401×10^{-8}–1.442×10^{-8}.

using the local log-slope is not independent of the presence and properties of another heterogeneity in another region of the medium. This phenomenon is expected since the long-term back-scattered photons used have the time of visiting the whole domain and hence each of the heterogeneities (even the farthest ones) before coming back and leading to a measurement. This is particularly true in Figs. 14 and 16 where it is seen that the effect of the difference in the properties of one of the heterogeneities (say absorption, picture (b)) on the corresponding reconstructions (picture (a)) cannot be decorrelated from the evolution of the properties of the other heterogeneities. For instance, the upper heterogeneity properties are the same in Figs. 14 and 16, however the reconstruction on Fig. 14 shows a higher level of the log-slopes product at the heterogeneity position compared to the level of the surroundings while the reconstruction in Fig. 16 exhibits a lower level. The only differences between both configurations are the optical properties of the other heterogeneity. Another illustration of this interdependence problem is the overall range of the log-slopes combination in the reconstructions: the relative contrast (identified in the figures by the "range of the relative log-slopes") is weaker for the phantoms where the heterogeneities have the same properties (Figs. 16 and 17). In this case, and in the contrary of Figs. 14 and 15, the overall optical properties of the medium (weighted mean of the background and of the heterogeneities properties) are changed owing to the uniform nature of the heterogeneities (pictures (b) and (c) in Figs. 16 and 17). The consequence is then an increase (or decrease) of the apparent medium properties, following the ones of the heterogeneities, so that the contrast in their optical effects with respect to this apparent background is relatively diminished. This interpretation concerning the lower relative range contrast of the reconstructions in Figs. 16 and 17 is valid only in the frame of an interaction between the whole area of the medium. The consequences of these conclusions are that, as with other direct imaging techniques and as specified in the introduction of the present paper, the access to the functional distribution is not allowed even if the inner structural configuration of the material is obtainable using the long term back-scattered photons.

In the particular configuration presented here, boundary effects are significant. It means that, even in the case of a homogeneous phantom, reflected signals at neighbouring nodes undergo different decaying. Fig. 18 illustrates those results with a time-dependent collection of back-scattered photons at the centre of an edge and at a distance corresponding to $8/25$ of its length from one of the square corners. It is seen that, due to boundary effects, there are long-scale variations along the boundary edge of the measured asymptotic log-slope. When heterogeneities are present in the material, superimposed short-scale variations are expected. Thus, data must be spatially decorrelated to obtain the short-scale information related to the presence of the heterogeneity and deconvolution spatial fil-

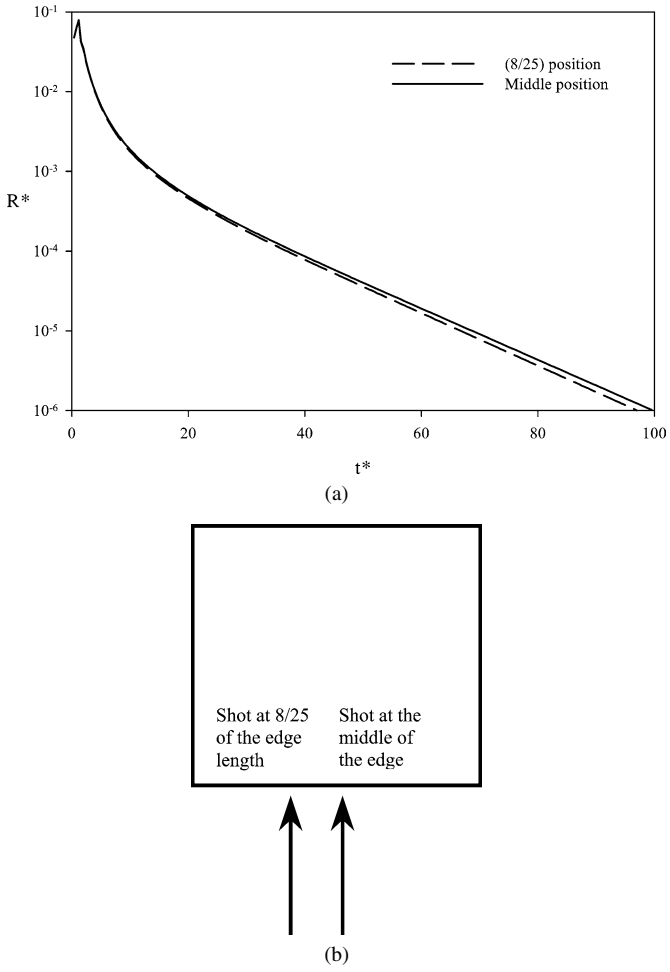

Fig. 18. Illustration of the boundary effects on the reflected signals. (a): Reflectance R^* signal recording as function of time t^*. (b): Location of two laser pulses at two neighbouring positions along one of the boundary edge.

tering seems to be necessary. In the cases presented in this paper, numerical simulations allow obtaining directly, at each node, the difference between the log-slopes generated by a non-homogeneous phantom and by the corresponding homogeneous phantom (what is called log-slopes in this paper is in fact these "relative log-slopes"). This facilitates the decorrelation and the interpretation of results. It should be noted however that a very recent experiment [31] conducted on a rectangular semi-transparent hexahedron of finite dimension with an embedded graphite heterogeneity, shows that the asymptotic log-slope of the back-scattered signal does not suffer from boundary effects in practice, due to the dimensions of real devices. In this latter study, reflectance log-slopes at different locations help localizing the position of the graphite inclusion in the deepness of the semi-transparent medium. This independent and parallel pioneering experimental work seems to confirm the methodology developed in the present paper.

5. Conclusion

Direct imaging presents several advantages compared to inverse reconstruction imaging. The set-up probing is relatively simple and images are fastly recovered directly throughout the process. Some drawbacks are also encountered: only structural information is available (optical properties are not recovered as such) and the probing is hitherto limited to thin media because of scattering events. Allowance for structural information only is an intrinsic limitation of the method; however it is sufficient in most diagnoses. In the contrary, present limitation to thin media severely precludes the availability of this very convenient and fast imaging technique.

A new imaging set-up has been studied in this paper in order to overcome the limitation on the optical thickness. For this, the remanent scattering signature itself is used to provide the contrast information building the images. In the first place, a detailed study of a generic three layered 1-D slab was able to highlight particular features, due to the presence of an inclusion, appearing in the emerging optical signals. As a consequence, a 2-D imaging technique was then proposed, assuming that observations on the 1-D slab are still reliable in a multi-D configuration.

The detailed parametrical study on the 1-D slab has shown that the asymptotic logarithmic slopes observed both in reflectance and transmittance are sensitive to the presence of an inclusion, its position and its optical nature. It is however impossible to distinguish the individual effects of position and optical properties for a given value of the log-slope. Furthermore, non-specificity has arisen for two symmetrical layering of the 1-D medium. However, this issue is unlikely to jeopardize adequate probing in practical situations since it seems to be rather strongly linked to particular 1-D configurations. This particular behaviour has been adapted to the 2-D case in order to locate the presence of heterogeneities embedded in a simple relatively thick phantom with the help of the back-scattered photons; the procedure may be generalized to the 3-D case. The imaging contrast is provided by the relative rate of change of the ALS and has the advantage of being independent of the knowledge of the optical properties. Furthermore, as the ALS is the key quantity, the method requires that the configuration exhibits this asymptotic regime of the readings. The new imaging technique proposed herein, numerically explored and which makes use of long-term back-scattered photons, seems to be confirmed by a very recent experiment [31], i.e. the relative difference in the reflected ALS along the surface is a potential tool for imaging (see, *interalia*, Figs. 3 and 4 [31] and the corresponding comments).

References

[1] Appl. Opt. 28 (12) (1989) (special issue).
[2] Appl. Opt. 30 (7) (1991) (special issue).
[3] Appl. Opt. 32 (4) (1993) (special issue).
[4] J. Boulanger, A. Charette, Numerical developments for short-pulsed near infra-red laser spectroscopy. Part I: direct treatment, J. Quant. Spectrosc. Radiat. Transfer 91 (2) (2005) 189–209.
[5] J. Boulanger, A. Charette, Numerical developments for short-pulsed near infra-red laser spectroscopy. Part II: inverse treatment, J. Quant. Spectrosc. Radiat. Transfer 91 (3) (2005) 297–318.
[6] V. Quaresima, M. Ferrari, M.C.P. van der Sluijs, J. Menssen, W.N.J.M. Colier, Lateral frontal cortex oxygenation changes during translation and language switching revealed by non-invasive near-infrared multi-point measurements, Brain Res. Bull. 59 (3) (2002) 235–243.

[7] B. Chance, C.E. Cooper, D.T. Delpy, E.O.R. Reynolds (Eds.), Near-infrared Spectroscopy and Imaging of Living Systems, Philos. Trans. Roy. Soc. London Ser. B 352 (1997).
[8] M.A. Franceschini, V. Toronov, M.E. Filiaci, E. Gratton, S. Fantini, On-line optical imaging of the human brain with 160-ms temporal resolution, Optics Express 6 (3) (2000) 49–57.
[9] W.F. Cheong, S.A. Prahl, A.J. Welch, A review of the optical properties of biological tissues, IEEE J. Quantum Electronics 26 (1990) 2166–2185.
[10] J.C. Hebden, K.S. Wong, Time resolved optical tomography, Appl. Opt. 32 (4) (1993) 372–380.
[11] R. Mahon, M.D. Duncan, L.L. Tankersley, J. Reintjes, Time-gated imaging through dense scatterers with a Raman amplifier, Appl. Opt. 32 (36) (1991) 7425–7433.
[12] D.T. Delpy, M. Cope, Pi. Van der Zee, S.R. Arridge, S. Wray, J. Wyatt, Estimation of optical pathlength through tissue from direct time of flight measurement, Phys. Med. Biol. 33 (12) (1988) 1433–1442.
[13] L. Wang, P.P. Ho, R.R. Alfano, Time-resolved Fourier spectrum and imaging in highly scattering media, Appl. Opt. 32 (26) (1993) 5043–5048.
[14] M.S. Patterson, B. Chance, B.C. Wilson, Time resolved reflectance and transmittance for the non-invasive measurement of tissue optical properties, Appl. Opt. 28 (12) (1989) 2331–2336.
[15] S.J. Madsen, B.C. Wilson, M.S. Patterson, Y.D. Park, S.L. Jacques, Y. Hefetz, Experimental tests of a simple diffusion model for the estimation of scattering and absorption coefficients of turbid media from time-resolved diffuse reflectance measurements, Appl. Opt. 31 (18) (1992) 3509–3517.
[16] M.Q. Brewster, Y. Yamada, Optical properties of thick turbid media from picosecond time-resolved light scattering measurements, Int. J. Heat Mass Transfer 38 (14) (1995) 2569–2581.
[17] A.H. Hielscher, H. Liu, B. Chance, F.K. Tittel, S.L. Jacques, Time-resolved photon emission from layered turbid media, Appl. Opt. 35 (4) (1996) 719–728.
[18] S.R. Arridge, J.C. Hebden, Optical imaging in medicine: II. Modelling and reconstruction, Phys. Med. Biol. 42 (5) (1997) 841–853.
[19] S.R. Arridge, Optical tomography in medical imaging, Inverse Problems 15 (2) (1999) 41–93.
[20] M.F. Modest, Radiative Heat Transfer, MacGraw-Hill, New York, ISBN 0-07-042675-9, 1993.
[21] A.A. Wray, Minimal storage time—advancement schemes of spectral methods, Technical Report, Center for Turbulence Research, Stanford University, Stanford, CA, 1990.
[22] F.J. Vesely, Computational Physics—An Introduction, second ed., Kluwer Academic/Plenum Publishers, New York/London, ISBN 0-306-46631-7, 2001.
[23] M.A. Ramankutty, A.L. Crosbie, Modified discrete ordinates method of radiative transfer in two-dimensional rectangular enclosures, J. Quant. Spectrosc. Radiat. Transfer 57 (1) (1997) 107–140.
[24] M. Sakami, A. Charette, Application of a modified discrete ordinates method to two-dimensional enclosures of irregular geometry, J. Quant. Spectrosc. Radiat. Transfer 64 (3) (2000) 275–298.
[25] M. Sakami, A. El Kasmi, A. Charette, Analysis of radiative heat transfer in complex two-dimensional enclosures with obstacles using the modified discrete ordinates method, ASME J. Heat Transfer 123 (5) (2001) 892–900.
[26] I. Ayranci, N. Selçuk, MOL solution of DOM for transient radiative transfer in 3-D scattering media, in: Proceedings of Eurotherm73 on Computational Thermal Radiation in Participating Media, Mons, Belgium, April 2003.
[27] P. Colella, P.R. Woodward, The piecewise parabolic method (PPM) for gas-dynamical simulations, J. Comput. Phys. 54 (1984) 174–201.
[28] J.M. Stone, D. Mihalas, Upwind monotonic interpolation methods for the solution of the time dependent radiative transfer equation, J. Comput. Phys. 100 (2) (1992) 402–408.
[29] M. Sakami, K. Mitra, P.-F. Hsu, Transient radiative transfer in anisotropically scattering media using monotonicity-preserving schemes, in: ASME HTD, vol. 366-1, ASME International ME Congress & Expo., Orlando, FL, 2000, pp. 135–143.
[30] M. Sakami, K. Mitra, P.-F. Hsu, Analysis of light pulse transport through two-dimensional scattering and absorbing media, J. Quant. Spectrosc. Radiat. Transfer 73 (2–5) (2002) 169–179.
[31] S.K. Wan, Z. Guo, S. Kumar, J. Aber, A. Garetz, Noninvasive detection of inhomogeneities in turbid media with time-resolved log-slope analysis, J. Quant. Spectrosc. Radiat. Transfer 84 (4) (2004) 493–500.
[32] J.C. Hebden, S.R. Arridge, D.T. Delpy, Optical imaging in medicine: I. Experimental techniques, Phys. Med. Biol. 42 (5) (1997) 825–840.